HHS Public Access

Author manuscript

Sci Immunol. Author manuscript; available in PMC 2020 December 05.

Published in final edited form as:

Sci Immunol. 2020 June 05; 5(48): . doi:10.1126/sciimmunol.abb1817.

T cell Engagement of Cross-Presenting Microglia Protects the Brain from a Nasal Virus Infection

E. Ashley Moseman[1,2,*], **Alexa C. Blanchard**[1,*], **Debasis Nayak**[3], **Dorian B. McGavern**[1]

[1]Viral Immunology & Intravital Imaging Section, National Institute of Neurological Disorders and Stroke, National Institutes of Health, Bethesda, MD

[2]Department of Immunology, Duke University School of Medicine, Durham, NC

[3]Discipline of Bioscience and Biomedical Engineering, Indian Institute of Technology Indore, MP, India

Abstract

The neuroepithelium is a nasal barrier surface populated by olfactory sensory neurons that detect odorants in the airway and convey this information directly to the brain via axon fibers. This barrier surface is especially vulnerable to infection, yet respiratory infections rarely cause fatal encephalitis, suggesting a highly evolved immunological defense. Here, using a mouse model, we sought to understand the mechanism by which innate and adaptive immune cells thwart neuroinvasion by vesicular stomatitis virus (VSV), a potentially lethal virus that uses olfactory sensory neurons to enter the brain after nasal infection. Fate-mapping studies demonstrated that infected CNS neurons were cleared non-cytolytically, yet specific deletion of MHC I from these neurons unexpectedly had no effect on viral control. Intravital imaging studies of calcium signaling in virus-specific CD8+ T cells revealed instead that brain resident microglia were the relevant source of viral peptide-MHC I complexes. Microglia were not infected by the virus but were found to cross-present antigen following acquisition from adjacent neurons. Microglia depletion interfered with T cell calcium signaling and antiviral control in the brain after nasal infection. Collectively, these data demonstrate that microglia provide a front-line defense against a neuroinvasive nasal infection by cross-presenting antigen to antiviral T cells that non-cytolytically cleanse neurons. Disruptions in this innate defense likely render the brain susceptible to neurotropic viruses like VSV that attempt to enter the CNS via the nose.

One Sentence Summary:

Microglia protect the brain from an intranasal VSV infection by cross-presenting neuronal antigen to antiviral CD8+ T cells.

Co-Corresponding Authors: Dorian B. McGavern, Ph.D., National Institutes of Health, Building 10, Room 5N240C, Bethesda, MD 20892, mcgavernd@mail.nih.gov, Phone: 301-443-7949; **Ashley Moseman, Ph.D.,** Duke University School of Medicine, 207 Research Drive, 101 Jones Building, Box 3010, Durham, NC 27710, ashley.moseman@duke.edu, Phone: 919-613-7811.

*Authors contributed equally to this manuscript.

AUTHOR CONTRIBUTIONS: A.C.B. and E.A.M. performed all the experiments and analyzed data. D.N. generated VSV recombinants. D.B.M. provided the funding. E.A.M. and D.B.M. wrote the manuscript.

COMPETING INTERESTS: The authors have no competing interests.

INTRODUCTION

Viral infections of the central nervous system (CNS) can be devastating when not properly contained (1, 2). Because the CNS contains irreplaceable post-mitotic cells, it is protected by several physical barriers that limit pathogen access into the CNS, including the blood brain barrier (BBB), blood cerebrospinal fluid barrier (B-CSF), and skull, among others. In addition, immune responses in this compartment are heavily regulated (3). Viruses in turn use several approaches to bypass these barriers such as direct infection of the BBB, invasion of peripheral nerves followed by transport into the CNS, and “trojan horse” entry via surveying immune cells (4). One especially vulnerable route that viruses use to invade the CNS is via olfactory sensory neurons (OSNs) within the nasal cavity.

OSNs lie within the mucosal upper airway surface, which is constantly exposed to environmental pathogens. However, the olfactory epithelium (OE) lining the nasal turbinates is unique in that this mucosal surface provides access for viruses to enter the CNS. Unlike the neighboring respiratory epithelium, the OE contains thousands to millions of OSNs (depending on the species) that are the predominant cell type within the olfactory neuroepithelial surface. While the OSN cell bodies lie beneath a layer of supporting or sustentacular cells, they extend a ciliated dendrite into the mucus lined airway space. Odorant information gathered from the external environment is conveyed via OSN axons within the turbinates through the specialized cribriform plate at the front of the skull and into the olfactory bulb of the brain (5). However, this anatomical arrangement also results in OSNs serving as a direct single cell route for neuroinvasion. Pathogens that infect OSNs can be shuttled intracellularly along OSN axons directly into the brain. The intracellular passage via OSNs into the brain allows invading pathogens to “tunnel under the castle wall” and evade classical CNS barriers that typically shield the brain. Thus, the olfactory route of infection is especially vulnerable to neurotropic viruses (6, 7).

The immune response to viruses must be appropriately balanced between pathogen clearance and limiting tissue damage. This balance is especially important in the CNS because most neurons are unable to regenerate, and damage can result in permanent damage to neural networks (1). While virus-induced cytopathology poses a serious concern to the CNS, immune-mediated cellular damage via perforin/granzyme poses a similar threat to neuronal integrity. Therefore, noncytolytic viral clearance via cytokines, especially interferons (IFNs), are believed to play an important role in CNS viral control (8-10). Type I interferons (IFN-I) are critical to the innate defense against most viruses (11) and also play an important role in priming adaptive immune responses (12, 13). On the other hand, IFNγ, which is primarily produced by lymphocytes (CD8+, CD4+, and NK cells) plays a dominant role in the control of CNS viral infections (14-17). TNFα has also been shown to facilitate non-cytolytic clearance (18-20).

Upper airway infections are a ubiquitous part of human life, and while many viruses infect the respiratory system (e.g. influenza, rhinovirus, coronavirus, respiratory syncytial virus), several of these viruses can also infect the olfactory epithelium. In this study, we used vesicular stomatitis virus (VSV) as a model for nasal infection because of its ability to target the olfactory epithelium preferentially over the respiratory epithelium (21) - a preference

shared by herpes simplex virus (HSV) (22). Several other viruses can also infect the olfactory epithelium, including mouse hepatitis virus (MHV) (23), parainfluenza (24), Japanese encephalitis virus (JEV) (25), and influenza virus (6, 26). Whereas seasonal influenza is typically an infection of respiratory epithelium (27), some more pathogenic strains are clearly able to target OSNs (26). Indeed, highly pathogenic avian influenza (HPAI) H5N1 prefers to replicate within the olfactory epithelium (28).

We undertook this study to better understand the mechanisms by which a cytopathic virus that infects the olfactory epithelium is contained and ultimately prohibited from spreading throughout the CNS. Intranasal VSV infection can induce a potent encephalitis that varies in outcome depending on the age and strain of the infected animal (29). Following nasal infection, VSV is transported from the airway via the olfactory epithelium into the CNS, where it initially is observed within the olfactory bulb (OB) (30). Virus replication is usually halted at the glomerular layer of the OB where OSN projections enter (10); however, the virus can sometimes move into deeper regions of the OB and throughout the CNS. VSV that escapes OSN-glomerular junction is believed to use retrograde axon transport as well as the ventricular system to move caudally in the CNS (31). It is known that IFN-I (32, 33), B cells (33, 34), and antiviral T cells (29, 35) all play a role in containing VSV. In this study, we monitored the in vivo activities of CD8+ T cells in the anatomical site where VSV is typically contained within the OB (glomeruli) and probed for the most functionally relevant source(s) of antigen presentation that result in non-cytolytic VSV control in neurons. Unexpectedly, an innate immune cell that is never infected by the virus (microglia) served as a key player in the control of virus in neurons.

RESULTS

Virus infection of the olfactory epithelial leads to rapid neuroinvasion

To more precisely understand how neurotropic viruses invade the CNS following infection of the olfactory epithelium (OE), we inoculated mice intranasally with VSV expressing DsRed (VSV-DsRed). This approach enabled us to monitor the distribution and spread of the virus in olfactory tissue. Confocal imaging of coronal whole head sections (Fig. S1) revealed 24 hrs after intranasal infection that there was widespread viral replication within olfactory sensory neurons (OSNs) in the OE (Fig. 1A,C). Following intranasal inoculation, VSV moves from the OE into the olfactory bulb (OB) where it is typically halted at the glomerular layer (10). At day 6 post-infection, we observed robust VSV-DsRed signal in outer nerve layer, which are peripheral nerves that project into the OB (Fig. 1B, D). We also observed virus in OB glomerular layer, indicating invasion of the brain parenchyma (Fig. 1B, D). Quantification of viral titers in the OB revealed VSV was very efficient at gaining access to the brain via this intranasal route (Fig. 1E). Viral titers reached ~10^4 plaque forming units (PFU) at 24 hours and climbed to ~10^5 PFU on day 6 before being extinguished by day 8.

To protect the CNS, noncytolytic viral clearance is often favored in this compartment (36). However, because VSV is a cytopathic virus, it was unclear whether this lifecycle could be halted once initiated. To determine if a cytopathic virus could be cleared non-cytolytically from the brain, we generated a recombinant of VSV expressing iCre-recombinase (VSV-

iCre). We then conducted fate-mapping studies by infecting floxed Stop TdTomato reporter ($Stop^{fl/fl}$ TdTomato) mice with this recombinant virus. Interestingly, we observed dense patches $TdTomato^+$ cells with a definitive neuronal morphology in the OB at late time points (>40 days) (Fig. 1F, S2), long after infectious virus was cleared from this compartment (Fig. 1E). These data indicate that VSV can be non-cytolytically cleared from the olfactory bulb, although it does not exclude the possibility that some cells are cytolytically cleared as well.

Intranasal VSV infection induces a robust immune response in the olfactory system

Except for patches of bone marrow within the turbinate bones, the naïve olfactory epithelium as shown in coronal head sections (Fig. S1A) contains few hematopoietic cells (Fig. 2A); however, after nasal infection, widespread VSV replication within the OE provoked robust inflammatory cell infiltration. $CD45^+$ leukocytes were observed in the OE as early as day 2, and infiltration elevated massively by day 6 post-infection (Fig. 2A). At this time point, virus and leukocytes were found in OE as well as the airways. This was associated with significant OE degradation and dissociation from the lamina propria (Fig. 2A,B).

Under steady state, the OB is defended in part by resident microglia; however, the arrival of VSV into this compartment via olfactory sensory neurons is associated with a large influx of peripherally-derived immune cells that surrounded infected glomeruli (Fig. 2A,C-E). This response was dominated by neutrophils and NK cells during the first 3 days, which were superseded by $CD8^+$ T cells and $Ly6C^{hi}$ monocytes at day 6 post-infection (Fig. 2E). $CD4^+$ T cells also arrived at this time point. At day 8 post-infection, T cell and monocyte numbers increased further within the OB (Fig. 2E). To track the recruitment of virus-specific $CD8^+$ T cells to the OB, we seeded mice intravenously with 3,000 $mCerulean^+$ OT-I and then infected them intranasally with VSV-OVA. VSV-specific $CD8^+$ T cells were primed and proliferated in the draining cervical lymph nodes and spleen and increased steadily over time in the OB (Fig. 2F). These data demonstrate that the OB mounts a robust immunological defense against intranasal VSV infection.

T cells and antiviral effector molecules protect against fatal VSV encephalitis

VSV titers in the OB are controlled between day 6 and 8 post-infection (Fig. 1E), which coincided with the arrival of antiviral T cells (Fig. 2E-F). We therefore sought to better understand the role of these T cells in preventing the fatal spread of VSV from olfactory glomeruli throughout the brain. We used survival rather than viral titers as an initial screen because we wanted to identify components of the OB antiviral defense that prevent induction of fatal disease after intranasal infection. Consistent with a previous study that used Balb/c mice (nu/nu) to demonstrate a role for T cells in controlling VSV (29), we found that a fraction of C57BL/6J mice depleted of either $CD8^+$ or $CD4^+$ T cells developed fatal VSV encephalitis (Fig. 3A). In addition, depletion of both T cell subsets induced fatal disease in nearly all mice infected intranasally with VSV. Consistent with this observation, we found increased viral titers in the OB (Fig. 3B) and caudal brain (Fig. 3C) of T cell depleted mice at day 8 post-infection. In addition, while VSV-GFP was largely confined to the outer nerve layer and glomeruli of control mice (Fig. 3D, F), T cell depletion promoted movement of VSV-GFP to other brain regions, including the rostral migratory stream and

brainstem (Fig. 3D, F). T cell depletion also allowed VSV-GFP to invade deeper layers of the OB, such as the mitral cell layer (Fig. 3E)

We next examined the effector mechanisms involved in preventing fatal VSV encephalitis. Mice deficient in tumor necrosis factor alpha (TNFα), interferon gamma (IFNγ), or perforin (PRF1) all showed modest reductions in survival comparable to that observed in mice depleted with anti-CD8 or CD4 antibodies (Fig. 3G). None of these knockout mice phenocopied the incidence of fatal disease observed in mice receiving anti-CD8/4 depleting antibodies (Fig. 3A). To determine if expression of the IFNγR was required on infected cells, we inoculated floxed IFNγR with VSV-iCre (Fig. 3H). This, however, did not reduce survival, indicating that IFNγR is not required on infected cells to elicit antiviral control. Collectively, these data suggest that there are redundant effector mechanisms controlling VSV within the OB.

Antiviral CTL have slowed motility within the infected OB

While it is likely, based on our depletion studies, that $CD4^+$ and $CD8^+$ T cells exert complementary antiviral programs following infection (Fig. 3A), we decided to focus in more detail on the $CD8^+$ T cell compartment because their MHC I restriction offered the possibility of studying a broader selection of potential target cells. We initially examined VSV-specific versus bystander $CD8^+$ T cell dynamics in the living OB at day 6 or 7 post-infection. We selected these time points because viral titers in the OB declined rapidly between day 6 and 8 post-infection (Fig. 1E), and we wanted to understand the mechanism by which this occurred. One day prior to VSV-OVA infection, B6 mice were seeded with 3,000 $mCerulean^+$ OT-I cells that served as the virus-specific $CD8^+$ T cell population. Bystander cells were generated by seeding a separate group of B6 mice with orange fluorescent protein $(OFP)^+$ P14 cells, which are specific to the glycoprotein of lymphocytic choriomeningitis virus (LCMV) (37). These mice were then infected intraperitoneally with LCMV Armstrong, and at day 7, effector OFP^+ P14 cells were harvested from the spleen and transferred into VSV-GFP-OVA infected mice one day prior to imaging. $mCerulean^+$ OT-I (VSV-specific) and OFP^+ P14 (bystander) cells were imaged simultaneously by intravital two-photon microscopy (TPM) through a thinned skull preparation (38, 39) made above the OB. This technique allowed us for the first time to analyze antiviral T cell behavior in the virally infected OB. Following VSV-GFP-OVA infection, virus-specific $CD8^+$ T cells moved rapidly along, between, and across infected axon tracts in the outer nerve layer as well as within the glomeruli (Fig. 4A,B; Movies S1-2). Quantification of T cell track velocities in two-photon time lapses revealed that virus-specific $CD8^+$ T cells had reduced track velocities relative to bystander T cells imaged in the same OB (Fig. 4C-D). In addition, virus-specific $CD8^+$ T cells also had a lower motility coefficient and higher arrest coefficient (Fig. 4D), all suggesting that these cells were encountering antigen locally (40).

CTL engage cognate antigen on an uninfected brain-resident cell population

To more accurately assess antigen encounters by virus-specific $CD8^+$ T cells in vivo, we devised an approach to monitor T cell calcium flux by TPM. T cell recognition of cognate peptide MHC complexes results in a rapid increase in intracellular calcium levels (41). We therefore generated OT-I and P14 cells expressing mTomato (to label the plasma membrane)

and GCaMP6s - a fluorescent calcium concentration indicator protein (13). Six days following intranasal infection with VSV-OVA, calcium flux was clearly visible in virus-specific $CD8^+$ T cells that had infiltrated and were surveying the OB (Fig. 5A,B,D; Movie S3). Calcium flux was rarely observed in infiltrating bystander P14 $CD8^+$ T cells indicating that T cell calcium flux is a good surrogate for cognate peptide MHC recognition (Fig. 5B) (13). We also observed that calcium fluxing virus-specific OT-I $CD8^+$ T cells had reduced instantaneous velocities relative to the cells that were not fluxing (Fig. 5C), which is consistent with studies showing that T cell antigen recognition is associated with decreased motility (40).

We next classified virus-specific $CD8^+$ T cell interactions in the virally infected OB into two groups based on velocity. “Kinetic” interactions were defined by continued T cell motility while fluxing calcium, whereas “stable” interactions were characterized by a relative loss of motility (<2 μm/min) during calcium flux (Fig. 5E-F; Movie S3) (42). Most antigen encounters (65%) by virus-specific $CD8^+$ T cells were defined as kinetic interactions. These cells did not arrest during peptide MHC recognition but paused briefly before continuing their migration through the OB (Fig. 5E-F; Movie S3). Virus-specific $CD8^+$ T cells also engaged in more stable interactions where the T cell would fully arrest and then flux calcium; however, this was only observed in 35% of the antigen encounters (Fig. 5E-F; Movie S3). Stable interactions typically resulted in more calcium fluxes (Fig. 5G) as well as longer flux durations relative to the kinetic interactions (Fig. S3).

Having defined the dynamics of virus-specific $CD8^+$ T cell interactions in the infected OB, we next sought to define target cell identity. In our imaging studies, we often noted that T cells would flux calcium upon engagement of “autofluorescent” cells (Fig. 5A,D; Movie S3). Morphologically, these autofluorescent cells did not match the size, shape, or spatial distribution of VSV-GFP infected cells that we typically observed in the OB. Because hematopoietic cells massively infiltrated the OB after VSV infection (Fig. 2), we posited that an infiltrating cell population might be responsible for presenting local antigen to virus-specific $CD8^+$ T cells. To address this possibility, we generated bone marrow chimeras in which the CNS resident compartment lacked MHC-I, whereas the infiltrating hematopoietic compartment was MHC-I sufficient. The percentage of donor-derived hematopoietic cells in the blood of these mice was 99.2 ± 0.4%, demonstrating near-complete chimerism. Strikingly, the overall frequency of CTL calcium flux dropped significantly in mice lacking MHC-I on the CNS resident compartment, indicating that antigen presentation to virus-specific CD8+ T cells relied primarily on a radiation resistant brain cell population rather than infiltrating hematopoietic cells (Fig. 5H). VSV is known to infect neurons, but MHC class I expression is expressed at very low levels on these cells (43, 44). We nevertheless set out to evaluate the importance cytotoxic lymphocyte (CTL)-neuronal interactions in controlling an intranasal VSV infection. To address this question, we generated a conditional beta-2 microglobulin mouse in which the exons 2 and 3 are flanked by loxP sites (floxed β2M) (Fig. S4A). β2M is an essential component of the MHC class I surface complex, and thus removal severely impairs presentation of class I peptides (45). We infected “conditional β2M” mice with VSV-iCre to remove the possibility that infected cells engage in direct antigen presentation to CD8+ T cells. Infection with VSV-iCre resulted in deletion of β2M from the genome of infected cells (Fig. S4B). However, unexpectedly, VSV-iCre infected

floxed β2M mice survived intranasal infection at the rate of control animals (Fig. 5I), indicating that the antiviral pressure exerted by CD8+ T cells, which is required in part for survival, does not involve direct interactions with virus-infected cells.

Microglia within the infected OB are activated and present antigen to CTL

Microglia are radiation resistant CNS resident myeloid cells, and while they are not believed to be potent antigen presenting cells in the naïve state (46), we characterized the surface expression of antigen presenting molecules on microglia during VSV infection (Fig. 6A,B). Six days following VSV infection, microglia in the OB showed evidence of activation characterized by robust upregulation of MHC class I, CD80 and CD86 as well as a very modest increase in CD40 and MHC II relative to naïve microglia (Fig. 6A-B). These changes in antigen presenting molecules suggested that microglia were capable of presenting viral antigen to CD8+ T cells.

We next sought to directly observe in vivo whether microglia were presenting antigen to virus-specific CD8+ T cells. To accomplish this, we adoptively transferred naïve mTomato+ GCaMP6s+ OT-I cells into bone marrow chimeras in which CX3CR1$^{gfp/+}$ were reconstituted with wild type bone marrow (99.6±0.31% blood chimerism). In these chimeras, radioresistant microglia are GFP positive, whereas all peripherally-derived hematopoietic cells as well as perivascular and meningeal macrophages are GFP negative. Six days following intranasal infection with VSV-OVA, we used intravital microscopy to identify calcium flux induced by antiviral CD8+ T cell engagement in the OB (Movie S4). We then quantified the frequency of CD8+ T cell antigen recognition (calcium flux) occurring in contact with microglia versus unlabeled space within the OB. This study revealed that ~72% of CD8+ T cell calcium flux occurred in contact with a CX3CR1$^{gfp/+}$ microglia (Fig. 6C,D; Movie S4), suggesting that microglia are indeed presenting cognate peptide MHC I complexes to virus-specific T cells. The interaction partner for the remaining CTL calcium flux events (~28%) is not known; however, it should be noted that the within the OB of the BM chimeras, 23.4±3.9% of the microglia were non-fluorescent (i.e., donor-derived). These cells might also have induced T cell calcium flux.

Microglia acquire infected OSN debris and orchestrate neuroprotective CTL activity

Our calcium imaging data suggested that microglia play an important role in presenting antigen to antiviral CD8+ T cells following VSV neuroinvasion. Neurons are the only known target of VSV following nasal infection; however, we decided to evaluate if microglia were also infected. We sought evidence for microglia infection in two ways - by inoculating wild type mice with VSV-GFP (Fig. S5A) and by inoculating Stop$^{fl/fl}$ TdTomato mice with VSV-iCre (Fig. S5B). Using either approach, flow cytometric analyses of the OB from infected mice revealed no evidence of microglia infection despite an abundance of virus in CD45 negative cells (presumably neurons) (Fig. S5A,B).

The absence of direct microglia infection led us to investigate alternative mechanisms of antigen acquisition and presentation by microglia. VSV can cause damage to the neurons it infects, and microglia are known to phagocytose cellular debris. We therefore evaluated whether microglia acquired antigen from VSV-infected OSNs. We labeled OSNs within the

OE by injecting fluorescent cholera toxin B (CTB) intranasally into OMP-GFP (Fig. S5C) or CX3CR1$^{gfp/+}$ mice (Fig. 7A) (47). Ten hours later, after CTB was transported along OSN axons into OB glomeruli (Fig. S5C), we infected mice with VSV and 6 days later observed clear evidence of CX3CR1$^{gfp/+}$ cells with intracellular CTB obtained from the labeled OSNs (Fig. 7A). These cells had the morphological characteristics of microglia, and this was confirmed flow cytometrically, which revealed that ~5% of microglia in the OB contained CTB (i.e., OSN debris) 6 days after infection (Fig. 7B, C). Processing the entire OB for flow cytometry, however, did not allow us to specifically analyze the anatomically relevant microglia in the glomerular layer of the OB, which is where VSV (Fig. 2C) and CTB (Fig. S5C) enter via OSN axons. We therefore quantified uptake histochemically, allowing us to focus on this anatomical site. We found 6 days after VSV infection that ~40% of Iba-1^{+} myeloid cells in OB glomeruli contained intracellular CTB derived from OSNs (Fig. 7D). For these studies, CTB served as a surrogate for an OSN-derived antigen. We next wanted to address whether microglia could also acquire virus particles. This was accomplished by infecting mice with VSV-PeGFP – a viral recombinant in which the phosphoprotein (P) is fused to eGFP enabling detection of the virion itself (48). Six days after infection with VSV-PeGFP, we determined that ~10% of Iba-1^{+} myeloid cells in OB glomeruli contained VSV-PeGFP (Fig. 7E). Collectively, these data indicate that microglia can directly acquire antigens from virally infected OSNs.

Having demonstrated that microglia could acquire OSN-derived antigens in vivo, we next asked whether their specific removal affected cognate antigen recognition of virus-specific CD8+ T cells in the infected OB. To deplete microglia, we first generated CX3CR1-Cre-ER x Rosa Stop$^{fl/fl}$ diphtheria toxin receptor (DTR) mice and treated them with tamoxifen to drive DTR expression in myeloid cells. After tamoxifen cessation, we waited an additional 60 days before DT treatment to allow for peripheral monocyte turnover (49). This is a commonly used approach that allows microglial depletion while preserving CX3CR1-expressing monocytes and antiviral T cells. These mice were then seeded with naïve mTomato+ GCaMP6s+ OT-I cells and infected intranasally with VSV-OVA. Six days later we observed that virus-specific CD8+ T cell calcium flux was significantly reduced in the microglia-depleted mice (Fig. 7F), indicating compromised viral antigen presentation when OB microglia but not monocytes were reduced (Fig. S6A,B). Interestingly, because the microglia depletion efficiency varied between animals, we tested whether there was any relationship between the frequency of CD8+ T cell calcium flux and the percentage of microglia remaining in the OB. Importantly, we observed a strong positive correlation ($r = 0.75$, $p < 0.0013$) between these two variables, further emphasizing the importance of microglia in fostering cognate antigen recognition and calcium flux in antiviral CD8+ T cells (Fig. 7G).

Lastly, we assessed the degree to which microglia contributed to the antiviral defense against an intranasal VSV infection. For this study, we used a more convenient alternative method to deplete microglia. Specifically, C57BL/6J mice were fed chow containing the CS1FR antagonist Pexidartinib (PLX3397) for 1-month (50). This treatment decreased the number of microglia in the OB by 66% without reducing the recruitment of CD8^{+} or CD8^{+} OT-I T cells in day 7 VSV-OVA infected mice (Fig. S6). Interestingly, despite the preservation of CD8^{+} T cells, VSV infection of PLX3397-treated animals resulted in frequent viral escape

at day 7 post-infection with elevated brain viral titers compared to control animals (Fig. 7H). Moreover, viral escape in PLX3397-treated mice was accompanied by reduced survival (Fig. 7I), which mirrored that observed in mice depleted of CD8+ T cells (Fig. 3G). Collectively, these data suggest that microglia can acquire and cross-present locally derived viral antigen to brain-infiltrating CD8+ T cells that exert antiviral pressure and contain VSV in the OB.

DISCUSSION

OSNs in the upper airway are responsible for relaying information about airborne odorants, but their contact with circulating air makes them a target for many pathogens. OSN infection provides a direct single cell route into the CNS that bypasses the classical blood brain barrier and blood CSF barriers. In this study, we sought novel insights into how the propagation of a cytopathic nasal pathogen is thwarted as it enters and attempts to spread throughout the CNS. Nasal VSV infection induced massive leukocyte infiltration into the OE. The virus nevertheless managed to travel via OSN axons through the cribriform plate and into the OB. Within the OB, fate-mapping studies revealed that VSV was controlled noncytolytically after infecting neurons in glomeruli as well as deeper neuronal layers. This containment depended in part on antiviral T cells and a combination of effector molecules (perforin, IFNγ, TNFα). However, specific removal of MHC I from virus-infected cells using floxed β2m mice demonstrated that direct engagement of neurons by CD8+ T cells was not required for viral control. This unexpected observation led us to perform intravital imaging studies of cognate antigen recognition by virus-specific CD8+ T cells in infected glomeruli. These studies revealed that microglia displayed cognate peptide-MHC I, promoting CTL antigen recognition and calcium flux. Importantly, microglia were not infected by VSV but instead acquired antigen from adjacent neurons, which was then cross-presented to the infiltrating virus-specific CTL. These interactions were functionally important, as microglia depletion markedly reduced cognate antigen recognition by CTL, impeding viral containment within the OB and promoting the development of fatal encephalitis.

Following nasal inoculation, virus is rapidly transported from the airway via the OSNs into the CNS where it is seen primarily within the OB. Viral replication is usually halted at the OSN-glomerular junction (10). Previous studies have shown that T cells play an important role in the control and clearance of VSV following CNS infection (29, 35). In addition, IFNγ, TNFα, IL-12, and nitric oxide synthase 1 were all shown to participate in the antiviral defense against VSV (51-55), yet is presently unclear how T cell effector functions are regulated in the CNS. Regulation of T cell effector functions is important because adult neurogenesis is reserved for specialized compartments (such as the OE (56, 57)); thus, when neurons are lost in the CNS during adulthood, they typically are not replaced. Because of this, it is postulated that the CNS favors the use of non-cytolytic viral clearance – a well described cytokine-mediated mechanism of eradicating an intracellular pathogen without killing the cell (18, 58). Cytokines such as IFNγ, TNFα, and IFN-I are all capable of purging viruses non-cytolytically, and this mode of viral clearance has been described for many different pathogens, including HBV (59), LCMV (60, 61), influenza virus (62, 63), MHV (64), and Sindis virus (65).

VSV is a cytopathic pathogen that is highly lytic in vitro (66); however, its interaction with the CNS appears to be more nuanced, as mice infected with VSV can sometimes harbor virus for several weeks before succumbing (Fig. 3G). While we cannot exclude a role for CTL using cytolytic effector molecules like perforin to control this virus (Fig. 3G), our fate mapping studies in VSV-iCre infected $Stop^{fl/fl}$ TdTomato reporter mice revealed ample evidence of previously infected OB neurons that were cleared non-cytolytically. These results are consistent with a previous study showing that neurotropic MHV can be non-cytolytically cleansed from OB interneurons following infection (64). Antiviral cytokines like IFNγ and TNFα are known to play a direct role in non-cytolytic viral clearance from the CNS (8, 9, 65) and peripheral tissues (18, 19, 60). We observed that both IFNγ- and TNFα-deficient mice have impaired survival following intranasal VSV infection, which is consistent with studies showing an important role for these cytokines in controlling other CNS infections. For example, IFNγ is known to help control measles virus (14), herpes virus (16), MHV (67), Borna virus (68), and recombinant vaccinia virus (69), whereas TNFα has a protective role against West Nile virus (WNV) (70), JEV (71), Tick-borne encephalitis virus (72), and HSV (73). In our study, VSV-iCre allowed us to distinguish the direct effects of IFNγ on infected cells from other potential functions exerted by this cytokine, such as the activation and recruitment of immune cells (74-76). Interestingly, we observed that IFNγR expression by infected cells plays no direct antiviral role in mediating survival after intranasal VSV inoculation. Whether TNFR is required on infected cells in this model is presently unclear.

MHC class I is important for different phases of normal brain development as well as for controlling ongoing plasticity (77, 78). However, MHC class I expression is often undetectable on most CNS neurons (43, 44, 79), and its ability to engage in physiologically relevant levels of antigen presentation is a source of continued debate. The classical paradigm suggests that activated CTL enter virally infected tissues and recognize cognate viral peptides presented in MHC class I molecules displayed on the infected cell surface. Indeed, following some viral infections, neuronal MHC I does appear to play a role in containing virus through CTL pressure, and these interactions can facilitate release of immune effector molecules and eventual neuronal damage (80). During HSV infection, CTL-derived IFNγ is believed to contribute to noncytolytic maintenance of viral latency within infected neurons (16, 81). In addition, perforin and granzyme B also participate in the noncytolytic control of this virus in neurons by degrading the HSV-1 immediate early protein (82). By contrast, CNS neurons infected by West Nile virus (WNV) are believed to be targeted directly by CTL that use perforin-mediated cytolytic mechanisms to purge virally infected neurons (83). It is presently unclear why some CTL engagements of infected neurons result in cytopathology, whereas others do not. This could be linked to the amount of MHC I expressed by different neuronal subtypes.

While CTL have the capacity to engage at least some virus-infected neuronal populations, our results in VSV-iCre infected floxed β2m mice demonstrate that MHC I expression on infected neurons does not play a role in protecting mice from fatal encephalitis (Fig. 5I). CTL are, however, important in preventing fatal disease after intranasal VSV infection (Fig. 5I), and our intravital imaging studies of cognate antigen recognition by antiviral CTL in the OB uncovered that microglia served as the target at least 70% of these interactions. This was

especially unexpected because we found no evidence, using two sensitive methods, that microglia were infected by VSV (Fig. S5B). These results suggested that microglia were in fact acquiring antigen from adjacent neurons and cross-presenting the material via MHC I to CTL. This conclusion is supported by our data showing that microglia within the OB engulfed the neuronal tracer CTB as well as fluorescent protein tagged VSV particles – a process that supplies potentially cross-presentable MHC I antigen. Cross-presentation is thought to be important during naïve CTL priming within secondary lymphoid organs; however, it can also occur in peripheral tissues, particularly tumors (84). In addition, both neonatal and adult microglia were previously shown to cross-present exogenous antigen (85), demonstrating that these cells do indeed have the capacity to cross-present.

Recent studies have begun to shed light on the roles microglia play in host defense and immunopathology after CNS virus infection (86-93). Depletion studies have revealed that microglia participate in the antiviral defense against pseudorabies virus (88), JEV (87), MHV (89), Theiler's murine encephalomyelitis virus (90), VSV (91), and WNV (87, 92). For example, Wheeler *et al.* found that many microglia-depleted mice fail to control MHV, resulting in compromised survival following intracerebral infection (89). This study also noted that microglia-depleted animals had impaired CD4+ T cell accumulation and function within the CNS. This is noteworthy because unlike microglia from VSV-infected brains (Fig. 6A) (94), MHV infection induces a marked upregulation of MHC II on microglia. These two models of virus infection appear to showcase an important functional divergence in the ability of microglia to support either MHC class I- or class II-restricted T cell responses in the virally-infected CNS. The importance of separating MHC I and II presentation to effector T cells in the CNS is not known; however, this is clearly the case following VSV infection, as OB-infiltrating myeloid cells express very high levels of MHC class II, whereas microglia do not (94).

While we did not focus on virus-specific CD4+ T cell interactions in this study, our findings demonstrate a clear role for cross-presenting microglia in displaying cognate peptide-MHC I complexes to CTL. We had intended to provide a more direct role for MHC I expression on microglia by conditionally deleting β2m from these cells. However, VSV infection of CX3CR1-Cre-ER x floxed β2m mice resulted in near complete NK cell-mediated deletion of the MHC I class negative microglia similar to what was described previously in inflamed floxed β2m mice (95). Nevertheless, our intravital imaging studies revealed that microglia supported most of the CTL calcium flux activity in the OB, and cognate antigen recognition was markedly reduced in their absence. In fact, CTL calcium flux in the infected OB correlated positively with the number of microglia remaining in depleted mice. In addition, microglia depletion promoted both viral escape into the brain and increased the incidence of fatal encephalitis. Antigen presentation by uninfected microglia to infiltrating CTL is likely a mechanism the CNS uses to elicit antiviral activity but protect neurons from direct CTL contact and potential lysis. It is also important to note that most CTL interactions with microglia were short-lived (kinetic) rather than stable. It is postulated that these short-lived interactions favor CTL usage of antiviral molecules (e.g. cytokines) rather than killing behavior (42). This would provide a mechanism to control virus in adjacent neurons without engaging them.

In conclusion, this study relied on intravital microscopy to analyze cognate antigen recognition by CTL as a nasal virus attempted to enter the brain via infection of the peripheral nervous system (i.e., OSNs). Because VSV primarily infects neurons, it was unclear how CTL would exert their antiviral pressure on a cell population that expresses little to no MHC I. However, our studies uncovered cross-presenting microglia as the main innate immune cell type responsible for driving protective, non-cytolytic CTL responses against a cytopathic CNS viral infection. These findings have important implications for our understanding of antiviral immunity, as they indicate that microglia need not be infected to present antigen in MHC I and participate in the eradication of virus from neurons. Evolutionarily, it makes sense for microglia to serve as an intermediary in the defense against a neuronal infection. Microglia are a renewable cell population, whereas most neurons are not. We therefore postulate that the CNS is designed to minimize direct engagement of infected neurons by CTL and favor release of non-cytolytic antiviral cytokines through interactions with cross-presenting intermediaries. Microglia play an important role in synaptic pruning as well as CNS homeostasis, and their proximity to neurons makes them an ideal candidate for this task. Given the role of microglia in cross-presenting viral antigen, factors that result in their distraction or depletion are likely to render the CNS more susceptible to infection.

Supplementary Material

Refer to Web version on PubMed Central for supplementary material.

ACKNOWLEDGMENTS:

We thank Alan Hoofring in the NIH Medical Arts Design Section for generating the illustration shown in Figure S1.

FUNDING: This research was supported by the intramural program at the National Institutes of Health.

REFERENCES

1. Swanson PA 2nd, McGavern DB, Viral diseases of the central nervous system. Curr Opin Virol 11, 44–54 (2015). [PubMed: 25681709]
2. Tyler KL, Acute Viral Encephalitis. N Engl J Med 379, 557–566 (2018). [PubMed: 30089069]
3. Forrester JV, McMenamin PG, Dando SJ, CNS infection and immune privilege. Nat Rev Neurosci 19, 655–671 (2018). [PubMed: 30310148]
4. McGavern DB, Kang SS, Illuminating viral infections in the nervous system. Nat Rev Immunol 11, 318–329 (2011). [PubMed: 21508982]
5. Barrios AW, Nunez G, Sanchez Quinteiro P, Salazar I, Anatomy, histochemistry, and immunohistochemistry of the olfactory subsystems in mice. Front Neuroanat 8, 63 (2014). [PubMed: 25071468]
6. van Riel D, Verdijk R, Kuiken T, The olfactory nerve: a shortcut for influenza and other viral diseases into the central nervous system. J Pathol 235, 277–287 (2015). [PubMed: 25294743]
7. Mori I, Nishiyama Y, Yokochi T, Kimura Y, Olfactory transmission of neurotropic viruses. J Neurovirol 11, 129–137 (2005). [PubMed: 16036791]
8. Binder GK, Griffin DE, Interferon-gamma-mediated site-specific clearance of alphavirus from CNS neurons. Science 293, 303–306 (2001). [PubMed: 11452126]
9. Burdeinick-Kerr R, Govindarajan D, Griffin DE, Noncytolytic clearance of sindbis virus infection from neurons by gamma interferon is dependent on Jak/STAT signaling. J Virol 83, 3429–3435 (2009). [PubMed: 19176616]

10. Detje CN, Meyer T, Schmidt H, Kreuz D, Rose JK, Bechmann I, Prinz M, Kalinke U, Local type I IFN receptor signaling protects against virus spread within the central nervous system. J Immunol 182, 2297–2304 (2009). [PubMed: 19201884]
11. McNab F, Mayer-Barber K, Sher A, Wack A, O'Garra A, Type I interferons in infectious disease. Nat Rev Immunol 15, 87–103 (2015). [PubMed: 25614319]
12. Crouse J, Kalinke U, Oxenius A, Regulation of antiviral T cell responses by type I interferons. Nat Rev Immunol 15, 231–242 (2015). [PubMed: 25790790]
13. Moseman EA, Wu T, de la Torre JC, Schwartzberg PL, McGavern DB, Type I interferon suppresses virus-specific B cell responses by modulating CD8(+) T cell differentiation. Sci Immunol 1, (2016).
14. Patterson CE, Lawrence DMP, Echols LA, Rall GF, Immune-mediated protection from measles virus-induced central nervous system disease is noncytolytic and gamma interferon dependent. J Virol 76, 4497–4506 (2002). [PubMed: 11932415]
15. Tishon A, Lewicki H, Andaya A, McGavern D, Martin L, Oldstone MBA, CD4 T cell control primary measles virus infection of the CNS: Regulation is dependent on combined activity with either CD8 T cells or with B cells: CD4, CD8 or B cells alone are ineffective. Virology 347, 234–245 (2006). [PubMed: 16529787]
16. Liu T, Khanna KM, Carriere BN, Hendricks RL, Gamma Interferon Can Prevent Herpes Simplex Virus Type 1 Reactivation from Latency in Sensory Neurons. J Virol 75, 11178–11184 (2001). [PubMed: 11602757]
17. Cantin EM, Hinton DR, Chen J, Openshaw H, Gamma interferon expression during acute and latent nervous system infection by herpes simplex virus type 1. J Virol 69, 4898–4905 (1995). [PubMed: 7609058]
18. Guidotti LG, Chisari FV, Noncytolytic control of viral infections by the innate and adaptive immune response. Annu Rev Immunol 19, 65–91 (2001). [PubMed: 11244031]
19. Gilles PN, Fey G, Chisari FV, Tumor necrosis factor alpha negatively regulates hepatitis B virus gene expression in transgenic mice. J Virol 66, 3955–3960 (1992). [PubMed: 1583737]
20. Lauterbach H, Zuniga EI, Truong P, Oldstone MB, McGavern DB, Adoptive immunotherapy induces CNS dendritic cell recruitment and antigen presentation during clearance of a persistent viral infection. J Exp Med 203, 1963–1975 (2006). [PubMed: 16847068]
21. Lundh B, Kristensson K, Norrby E, Selective infections of olfactory and respiratory epithelium by vesicular stomatitis and Sendai viruses. Neuropathol Appl Neurobiol 13, 111–122 (1987). [PubMed: 3039392]
22. Shivkumar M, Milho R, May JS, Nicoll MP, Efstathiou S, Stevenson PG, Herpes simplex virus 1 targets the murine olfactory neuroepithelium for host entry. J Virol 87, 10477–10488 (2013). [PubMed: 23903843]
23. Barnett EM, Perlman S, The olfactory nerve and not the trigeminal nerve is the major site of CNS entry for mouse hepatitis virus, strain JHM. Virology 194, 185–191 (1993). [PubMed: 8386871]
24. Mori I, Komatsu T, Takeuchi K, Nakakuki K, Sudo M, Kimura Y, Parainfluenza virus type 1 infects olfactory neurons and establishes long-term persistence in the nerve tissue. J Gen Virol 76 (Pt 5), 1251–1254 (1995). [PubMed: 7730810]
25. Park SL, Huang YS, Lyons AC, Ayers VB, Hettenbach SM, McVey DS, Burton KR, Higgs S, Vanlandingham DL, North American domestic pigs are susceptible to experimental infection with Japanese encephalitis virus. Sci Rep 8, 7951 (2018). [PubMed: 29784969]
26. Mori I, Goshima F, Imai Y, Kohsaka S, Sugiyama T, Yoshida T, Yokochi T, Nishiyama Y, Kimura Y, Olfactory receptor neurons prevent dissemination of neurovirulent influenza A virus into the brain by undergoing virus-induced apoptosis. J Gen Virol 83, 2109–2116 (2002). [PubMed: 12185263]
27. van den Brand JM, Stittelaar KJ, van Amerongen G, Reperant L, de Waal L, Osterhaus AD, Kuiken T, Comparison of temporal and spatial dynamics of seasonal H3N2, pandemic H1N1 and highly pathogenic avian influenza H5N1 virus infections in ferrets. PLoS One 7, e42343 (2012). [PubMed: 22905124]
28. Schrauwen EJ, Herfst S, Leijten LM, van Run P, Bestebroer TM, Linster M, Bodewes R, Kreijtz JH, Rimmelzwaan GF, Osterhaus AD, Fouchier RA, Kuiken T, van Riel D, The multibasic

cleavage site in H5N1 virus is critical for systemic spread along the olfactory and hematogenous routes in ferrets. J Virol 86, 3975–3984 (2012). [PubMed: 22278228]

29. Huneycutt BS, Bi Z, Aoki CJ, Reiss CS, Central neuropathogenesis of vesicular stomatitis virus infection of immunodeficient mice. J Virol 67, 6698–6706 (1993). [PubMed: 8105106]
30. Reiss CS, Plakhov IV, Komatsu T, Viral replication in olfactory receptor neurons and entry into the olfactory bulb and brain. Ann N Y Acad Sci 855, 751–761 (1998). [PubMed: 9929681]
31. Cornish TE, Stallknecht DE, Brown CC, Seal BS, Howerth EW, Pathogenesis of experimental vesicular stomatitis virus (New Jersey serotype) infection in the deer mouse (Peromyscus maniculatus). Vet Pathol 38, 396–406 (2001). [PubMed: 11467473]
32. Muller U, Steinhoff U, Reis LF, Hemmi S, Pavlovic J, Zinkernagel RM, Aguet M, Functional role of type I and type II interferons in antiviral defense. Science 264, 1918–1921 (1994). [PubMed: 8009221]
33. Steinhoff U, Müller U, Schertler A, Hengartner H, Aguet M, Zinkernagel RM, Antiviral protection by vesicular stomatitis virus-specific antibodies in alpha/beta interferon receptor-deficient mice. J Virol 69, 2153–2158 (1995). [PubMed: 7884863]
34. Moseman EA, Iannacone M, Bosurgi L, Tonti E, Chevrier N, Tumanov A, Fu YX, Hacohen N, von Andrian UH, B cell maintenance of subcapsular sinus macrophages protects against a fatal viral infection independent of adaptive immunity. Immunity 36, 415–426 (2012). [PubMed: 22386268]
35. Reiss C, Aoki C, Vesicular stomatitis virus: Immune recognition, responsiveness, and pathogenesis of infection in mice. Rev Med Virol 4, 129–140 (1994).
36. Griffin DE, Metcalf T, Clearance of virus infection from the CNS. Curr Opin Immunol 1, 216–221 (2011).
37. Pircher H, Burki K, Lang R, Hengartner H, Zinkernagel RM, Tolerance induction in double specific T-cell receptor transgenic mice varies with antigen. Nature 342, 559–561 (1989). [PubMed: 2573841]
38. Yang G, Pan F, Parkhurst CN, Grutzendler J, Gan WB, Thinned-skull cranial window technique for long-term imaging of the cortex in live mice. Nat Protoc 5, 201–208 (2010). [PubMed: 20134419]
39. Manglani M, McGavern DB, Intravital Imaging of Neuroimmune Interactions Through a Thinned Skull. Curr Protoc Immunol 120, 24 22 21–24 22 12 (2018).
40. Moreau HD, Lemaitre F, Garrod KR, Garcia Z, Lennon-Dumenil AM, Bousso P, Signal strength regulates antigen-mediated T-cell deceleration by distinct mechanisms to promote local exploration or arrest. Proc Natl Acad Sci U S A 112, 12151–12156 (2015). [PubMed: 26371316]
41. Oh-hora M, Rao A, Calcium signaling in lymphocytes. Curr Opin Immunol 20, 250–258 (2008). [PubMed: 18515054]
42. Fooksman DR, Vardhana S, Vasiliver-Shamis G, Liese J, Blair DA, Waite J, Sacristan C, Victora GD, Zanin-Zhorov A, Dustin ML, Functional anatomy of T cell activation and synapse formation. Annu Rev Immunol 28, 79–105 (2010). [PubMed: 19968559]
43. Joly E, Mucke L, Oldstone MB, Viral persistence in neurons explained by lack of major histocompatibility class I expression. Science 253, 1283–1285 (1991). [PubMed: 1891717]
44. Joly E, Oldstone MB, Neuronal cells are deficient in loading peptides onto MHC class I molecules. Neuron 8, 1185–1190 (1992). [PubMed: 1610569]
45. Koller BH, Marrack P, Kappler JW, Smithies O, Normal development of mice deficient in beta 2M, MHC class I proteins, and CD8+ T cells. Science 248, 1227–1230 (1990). [PubMed: 2112266]
46. Nayak D, Roth TL, McGavern DB, Microglia development and function. Annu Rev Immunol 32, 367–402 (2014). [PubMed: 24471431]
47. van Ginkel FW, Jackson RJ, Yuki Y, McGhee JR, Cutting edge: the mucosal adjuvant cholera toxin redirects vaccine proteins into olfactory tissues. J Immunol 165, 4778–4782 (2000). [PubMed: 11045998]
48. Das SC, Nayak D, Zhou Y, Pattnaik AK, Visualization of intracellular transport of vesicular stomatitis virus nucleocapsids in living cells. J Virol 80, 6368–6377 (2006). [PubMed: 16775325]
49. Parkhurst CN, Yang G, Ninan I, Savas JN, Yates JR 3rd, Lafaille JJ, Hempstead BL, Littman DR, Gan WB, Microglia promote learning-dependent synapse formation through brain-derived neurotrophic factor. Cell 155, 1596–1609 (2013). [PubMed: 24360280]

50. Elmore MR, Najafi AR, Koike MA, Dagher NN, Spangenberg EE, Rice RA, Kitazawa M, Matusow B, Nguyen H, West BL, Green KN, Colony-stimulating factor 1 receptor signaling is necessary for microglia viability, unmasking a microglia progenitor cell in the adult brain. Neuron 82, 380–397 (2014). [PubMed: 24742461]
51. Bi Z, Barna M, Komatsu T, Reiss CS, Vesicular stomatitis virus infection of the central nervous system activates both innate and acquired immunity. J Virol 69, 6466–6472 (1995). [PubMed: 7545248]
52. Bi Z, Reiss CS, Inhibition of vesicular stomatitis virus infection by nitric oxide. J Virol 69, 2208–2213 (1995). [PubMed: 7533852]
53. Komatsu T, Ireland DDC, Chen N, Reiss CS, Neuronal expression of NOS-1 is required for host recovery from viral encephalitis. Virology 258, 389–395 (1999). [PubMed: 10366576]
54. Komatsu T, Bi Z, Reiss CS, Interferon-gamma induced type I nitric oxide synthase activity inhibits viral replication in neurons. J Neuroimmunol 68, 101–108 (1996). [PubMed: 8784266]
55. Komatsu T, Barna M, Reiss CS, Interleukin-12 promotes recovery from viral encephalitis. Viral Immunol 10, 35–47 (1997). [PubMed: 9095530]
56. Leung CT, Coulombe PA, Reed RR, Contribution of olfactory neural stem cells to tissue maintenance and regeneration. Nat Neurosci 10, 720–726 (2007). [PubMed: 17468753]
57. Schwob JE, Neural regeneration and the peripheral olfactory system. Anat Rec 269, 33–49 (2002). [PubMed: 11891623]
58. Guidotti LG, Chisari FV, Cytokine-induced viral purging--role in viral pathogenesis. Curr Opin Microbiol 2, 388–391 (1999). [PubMed: 10490351]
59. Guidotti LG, Rochford R, Chung J, Shapiro M, Purcell R, Chisari FV, Viral clearance without destruction of infected cells during acute HBV infection. Science 284, 825–829 (1999). [PubMed: 10221919]
60. Guidotti LG, Borrow P, Brown A, McClary H, Koch R, Chisari FV, Noncytopathic clearance of lymphocytic choriomeningitis virus from the hepatocyte. J Exp Med 189, 1555–1564 (1999). [PubMed: 10330434]
61. Herz J, Johnson KR, McGavern DB, Therapeutic antiviral T cells noncytopathically clear persistently infected microglia after conversion into antigen-presenting cells. J Exp Med 212, 1153–1169 (2015). [PubMed: 26122661]
62. Heaton NS, Langlois RA, Sachs D, Lim JK, Palese P, tenOever BR, Long-term survival of influenza virus infected club cells drives immunopathology. J Exp Med 211, 1707–1714 (2014). [PubMed: 25135297]
63. Dumm RE, Fiege JK, Waring BM, Kuo CT, Langlois RA, Heaton NS, Non-lytic clearance of influenza B virus from infected cells preserves epithelial barrier function. Nat Commun 10, 779 (2019). [PubMed: 30770807]
64. Wheeler DL, Athmer J, Meyerholz DK, Perlman S, Murine Olfactory Bulb Interneurons Survive Infection with a Neurotropic Coronavirus. J Virol 91, (2017).
65. Burdeinick-Kerr R, Griffin DE, Gamma interferon-dependent, noncytolytic clearance of sindbis virus infection from neurons in vitro. J Virol 79, 5374–5385 (2005). [PubMed: 15827152]
66. Faulkner G, Dubois-Dalcq M, Hooghe-Peters E, McFarland HF, Lazzarini RA, Defective interfering particles modulate VSV infection of dissociated neuron cultures. Cell 17, 979–991 (1979). [PubMed: 226268]
67. Pearce BD, Hobbs MV, McGraw TS, Buchmeier MJ, Cytokine induction during T-cell-mediated clearance of mouse hepatitis virus from neurons in vivo. J Virol 68, 5483–5495 (1994). [PubMed: 8057431]
68. Hausmann J, Pagenstecher A, Baur K, Richter K, Rziha HJ, Staeheli P, CD8 T cells require gamma interferon to clear borna disease virus from the brain and prevent immune system-mediated neuronal damage. J Virol 79, 13509–13518 (2005). [PubMed: 16227271]
69. Kundig TM, Hengartner H, Zinkernagel RM, T cell-dependent IFN-gamma exerts an antiviral effect in the central nervous system but not in peripheral solid organs. J Immunol 150, 2316–2321 (1993). [PubMed: 8450214]

70. Shrestha B, Zhang B, Purtha WE, Klein RS, Diamond MS, Tumor necrosis factor alpha protects against lethal West Nile virus infection by promoting trafficking of mononuclear leukocytes into the central nervous system. J Virol 82, 8956–8964 (2008). [PubMed: 18632856]
71. Hayasaka D, Shirai K, Aoki K, Nagata N, Simantini DS, Kitaura K, Takamatsu Y, Gould E, Suzuki R, Morita K, TNF-alpha acts as an immunoregulator in the mouse brain by reducing the incidence of severe disease following Japanese encephalitis virus infection. PLoS One 8, e71643 (2013). [PubMed: 23940775]
72. Tun MM, Aoki K, Senba M, Buerano CC, Shirai K, Suzuki R, Morita K, Hayasaka D, Protective role of TNF-alpha, IL-10 and IL-2 in mice infected with the Oshima strain of Tick-borne encephalitis virus. Sci Rep 4, 5344 (2014). [PubMed: 24938868]
73. Sergerie Y, Rivest S, Boivin G, Tumor necrosis factor-alpha and interleukin-1 beta play a critical role in the resistance against lethal herpes simplex virus encephalitis. J Infect Dis 196, 853–860 (2007). [PubMed: 17703415]
74. Zhang X, Hinton DR, Cua DJ, Stohlman SA, Lai MM, Expression of interferon-gamma by a coronavirus defective-interfering RNA vector and its effect on viral replication, spread, and pathogenicity. Virology 233, 327–338 (1997). [PubMed: 9217056]
75. Liu MT, Armstrong D, Hamilton TA, Lane TE, Expression of Mig (monokine induced by interferon-gamma) is important in T lymphocyte recruitment and host defense following viral infection of the central nervous system. J Immunol 166, 1790–1795 (2001). [PubMed: 11160225]
76. Lin AA, Tripathi PK, Sholl A, Jordan MB, Hildeman DA, Gamma interferon signaling in macrophage lineage cells regulates central nervous system inflammation and chemokine production. J Virol 83, 8604–8615 (2009). [PubMed: 19515766]
77. Huh GS, Boulanger LM, Du H, Riquelme PA, Brotz TM, Shatz CJ, Functional requirement for class I MHC in CNS development and plasticity. Science 290, 2155–2159 (2000). [PubMed: 11118151]
78. Elmer BM, McAllister AK, Major histocompatibility complex class I proteins in brain development and plasticity. Trends Neurosci 35, 660–670 (2012). [PubMed: 22939644]
79. Rall GF, CNS neurons: the basis and benefits of low class I major histocompatibility complex expression. Curr Top Microbiol Immunol 232, 115–134 (1998). [PubMed: 9557396]
80. Chevalier G, Suberbielle E, Monnet C, Duplan V, Martin-Blondel G, Farrugia F, Le Masson G, Liblau R, Gonzalez-Dunia D, Neurons are MHC class I-dependent targets for CD8 T cells upon neurotropic viral infection. PLoS Pathog 7, e1002393 (2011). [PubMed: 22114563]
81. Liu T, Khanna KM, Chen X, Fink DJ, Hendricks RL, CD8(+) T cells can block herpes simplex virus type 1 (HSV-1) reactivation from latency in sensory neurons. J Exp Med 191, 1459–1466 (2000). [PubMed: 10790421]
82. Knickelbein JE, Khanna KM, Yee MB, Baty CJ, Kinchington PR, Hendricks RL, Noncytotoxic lytic granule-mediated CD8+ T cell inhibition of HSV-1 reactivation from neuronal latency. Science 322, 268–271 (2008). [PubMed: 18845757]
83. Shrestha B, Samuel MA, Diamond MS, CD8+ T cells require perforin to clear West Nile virus from infected neurons. J Virol 80, 119–129 (2006). [PubMed: 16352536]
84. Cruz FM, Colbert JD, Merino E, Kriegsman BA, Rock KL, The Biology and Underlying Mechanisms of Cross-Presentation of Exogenous Antigens on MHC-I Molecules. Annu Rev Immunol 35, 149–176 (2017). [PubMed: 28125356]
85. Beauvillain C, Donnou S, Jarry U, Scotet M, Gascan H, Delneste Y, Guermonprez P, Jeannin P, Couez D, Neonatal and adult microglia cross-present exogenous antigens. Glia 56, 69–77 (2008). [PubMed: 17932942]
86. Vasek MJ, Garber C, Dorsey D, Durrant DM, Bollman B, Soung A, Yu J, Perez-Torres C, Frouin A, Wilton DK, Funk K, DeMasters BK, Jiang X, Bowen JR, Mennerick S, Robinson JK, Garbow JR, Tyler KL, Suthar MS, Schmidt RE, Stevens B, Klein RS, A complement-microglial axis drives synapse loss during virus-induced memory impairment. Nature 534, 538–543 (2016). [PubMed: 27337340]
87. Seitz S, Clarke P, Tyler KL, Pharmacologic Depletion of Microglia Increases Viral Load in the Brain and Enhances Mortality in Murine Models of Flavivirus-Induced Encephalitis. J Virol 92, (2018).

88. Fekete R, Cserep C, Lenart N, Toth K, Orsolits B, Martinecz B, Mehes E, Szabo B, Nemeth V, Gonci B, Sperlagh B, Boldogkoi Z, Kittel A, Baranyi M, Ferenczi S, Kovacs K, Szalay G, Rozsa B, Webb C, Kovacs GG, Hortobagyi T, West BL, Kornyei Z, Denes A, Microglia control the spread of neurotropic virus infection via P2Y12 signalling and recruit monocytes through P2Y12-independent mechanisms. Acta Neuropathol 136, 461–482 (2018). [PubMed: 30027450]

89. Wheeler DL, Sariol A, Meyerholz DK, Perlman S, Microglia are required for protection against lethal coronavirus encephalitis in mice. J Clin Invest 128, 931–943 (2018). [PubMed: 29376888]

90. Waltl I, Kaufer C, Gerhauser I, Chhatbar C, Ghita L, Kalinke U, Loscher W, Microglia have a protective role in viral encephalitis-induced seizure development and hippocampal damage. Brain Behav Immun 74, 186–204 (2018). [PubMed: 30217535]

91. Chhatbar C, Detje CN, Grabski E, Borst K, Spanier J, Ghita L, Elliott DA, Jordao MJC, Mueller N, Sutton J, Prajeeth CK, Gudi V, Klein MA, Prinz M, Bradke F, Stangel M, Kalinke U, Type I Interferon Receptor Signaling of Neurons and Astrocytes Regulates Microglia Activation during Viral Encephalitis. Cell Rep 25, 118–129 e114 (2018). [PubMed: 30282022]

92. Funk KE, Klein RS, CSF1R antagonism limits local restimulation of antiviral CD8(+) T cells during viral encephalitis. J Neuroinflammation 16, 22 (2019). [PubMed: 30704498]

93. Garber C, Soung A, Vollmer LL, Kanmogne M, Last A, Brown J, Klein RS, T cells promote microglia-mediated synaptic elimination and cognitive dysfunction during recovery from neuropathogenic flaviviruses. Nat Neurosci 22, 1276–1288 (2019). [PubMed: 31235930]

94. D'Agostino PM, Kwak C, Vecchiarelli HA, Toth JG, Miller JM, Masheeb Z, McEwen BS, Bulloch K, Viral-induced encephalitis initiates distinct and functional CD103+ CD11b+ brain dendritic cell populations within the olfactory bulb. Proc Natl Acad Sci U S A 109, 6175–6180 (2012). [PubMed: 22474352]

95. Bern MD, Parikh BA, Yang L, Beckman DL, Poursine-Laurent J, Yokoyama WM, Inducible down-regulation of MHC class I results in natural killer cell tolerance. J Exp Med 216, 99–116 (2019). [PubMed: 30559128]

96. Perarnau B, Saron MF, Reina San Martin B, Bervas N, Ong H, Soloski MJ, Smith AG, Ure JM, Gairin JE, Lemonnier FA, Single H2Kb, H2Db and double H2KbDb knockout mice: peripheral CD8+ T cell repertoire and anti-lymphocytic choriomeningitis virus cytolytic responses. Eur J Immunol 29, 1243–1252 (1999). [PubMed: 10229092]

97. Gossa S, Nayak D, Zinselmeyer BH, McGavern DB, Development of an immunologically tolerated combination of fluorescent proteins for in vivo two-photon imaging. Sci Rep 4, 6664 (2014). [PubMed: 25322934]

98. Potter SM, Zheng C, Koos DS, Feinstein P, Fraser SE, Mombaerts P, Structure and emergence of specific olfactory glomeruli in the mouse. J Neurosci 21, 9713–9723 (2001). [PubMed: 11739580]

99. Kim SK, Reed DS, Olson S, Schnell MJ, Rose JK, Morton PA, Lefrancois L, Generation of mucosal cytotoxic T cells against soluble protein by tissue-specific environmental and costimulatory signals. Proc Natl Acad Sci U S A 95, 10814–10819 (1998). [PubMed: 9724787]

100. Chandran K, Sullivan NJ, Felbor U, Whelan SP, Cunningham JM, Endosomal proteolysis of the Ebola virus glycoprotein is necessary for infection. Science 308, 1643–1645 (2005). [PubMed: 15831716]

101. Shimshek DR, Kim J, Hubner MR, Spergel DJ, Buchholz F, Casanova E, Stewart AF, Seeburg PH, Sprengel R, Codon-improved Cre recombinase (iCre) expression in the mouse. Genesis 32, 19–26 (2002). [PubMed: 11835670]

102. Zinselmeyer BH, Dempster J, Wokosin DL, Cannon JJ, Pless R, Parker I, Miller MJ, Chapter 16. Two-photon microscopy and multidimensional analysis of cell dynamics. Methods Enzymol 461, 349–378 (2009). [PubMed: 19480927]

103. Susaki EA, Tainaka K, Perrin D, Yukinaga H, Kuno A, Ueda HR, Advanced CUBIC protocols for whole-brain and whole-body clearing and imaging. Nat Protoc 10, 1709–1727 (2015). [PubMed: 26448360]

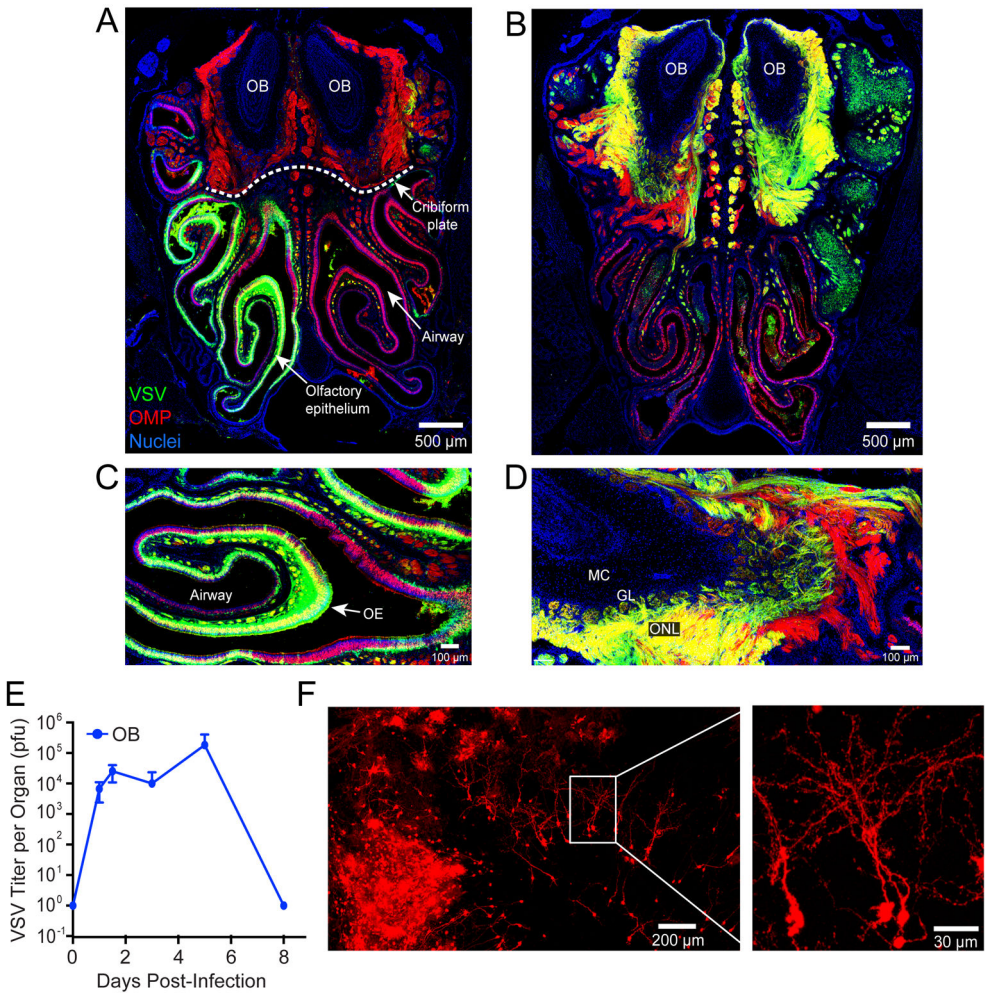

Figure 1. VSV rapidly travels from the nasal turbinates into the OB where it is controlled noncytolytically.

A,B) Representative confocal micrographs of coronal head sections (see Figure S1) show the nasal airway, olfactory epithelium (OE), cribriform plate (dotted white line), and olfactory bulbs (OB) from OMP-GFP mice on days 1 (A) and 6 (B) post-intranasal VSV-DsRed (green) infection (OMP-GFP in red, nuclei shown in blue). C,D) Higher magnification images show the virus invading the OE at day 1 (C) and OB via the outer nerve layer at day 6 (D). Anatomical structures such as the airway, OE, olfactory nerve layer (ONL), glomerular layer (GL), and mitral cell layer (ML) are annotated in these images. E) Time course of viral titers represented as plaque forming units (pfu) per OB following intranasal VSV infection (mean±SD; n=4-5 mice per timepoint; data representative of 3 independent experiments). F) Confocal micrographs of a cleared olfactory bulb from a VSV-iCre infected $Stop^{fl/fl}$ tdTomato reporter mouse 50 days post-intranasal infection.

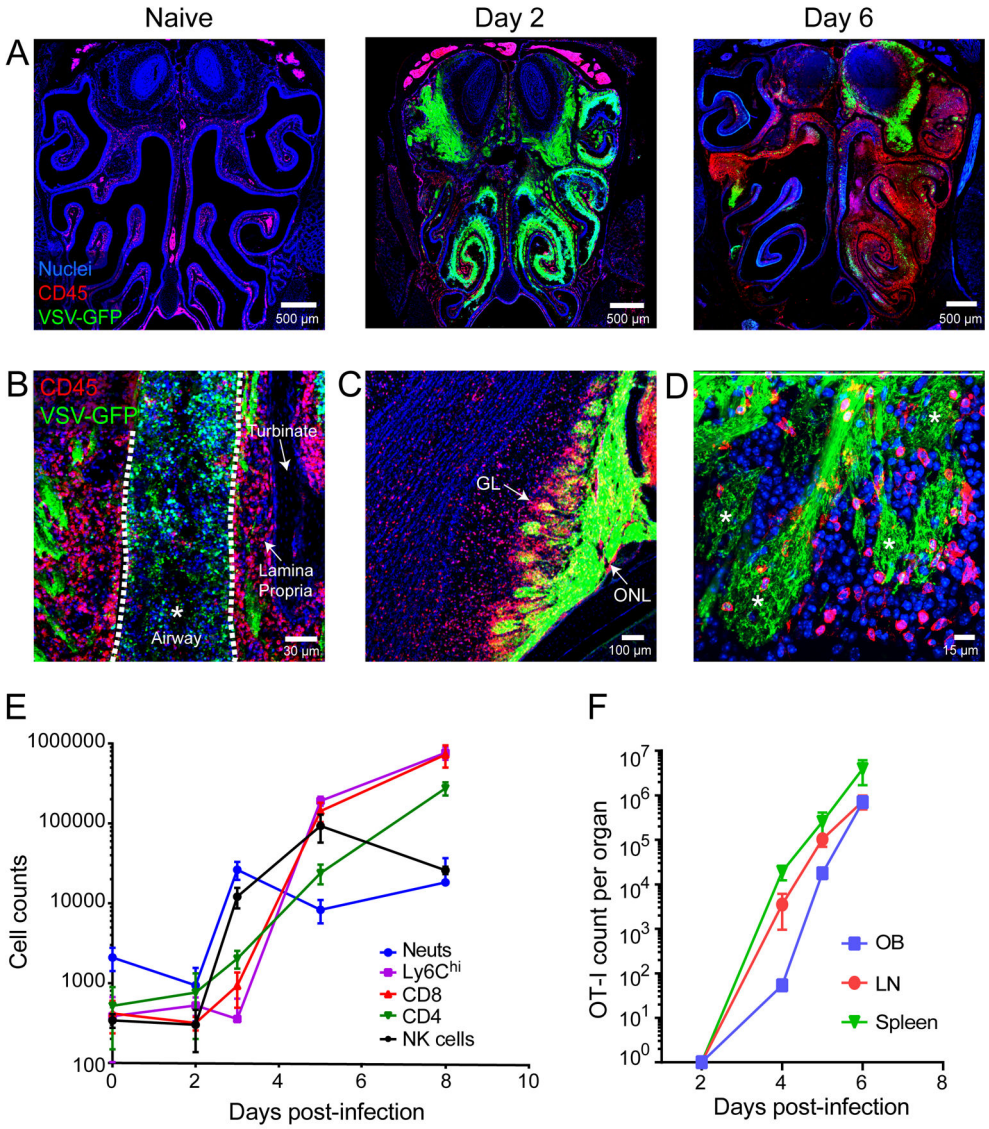

Figure 2. Intranasal VSV infection drives massive immune cell infiltration into the OE and OB.

A) Representative confocal images of coronal head sections (see Figure S1) show the distribution of CD45+ leukocytes (red) in OE / OB uninfected mice relative to day 2 and day 6 post-intranasal VSV-GFP (green) infection. Cell nuclei are shown in blue. B) Confocal micrograph depicting CD45+ infiltration into the VSV-eGFP infected olfactory turbinates 6 days post-infection. Note that the airway space denoted with white asterisk and dotted white lines is filled with cells and virus. C) A confocal micrograph from a day 6 infected OB shows VSV-GFP in the glomerular layer (GL) and outer nerve layer (ONL). D) Confocal micrograph of day6 VSV-eGFP infected OSN terminals. Asterisks denote individual glomeruli within the OB. E) Graph depicts the kinetics of inflammatory cell infiltration into the VSV infected OB. The following markers were used to identify the different immune subsets after first gating on LIVE, CD45+ cells: neutrophils ($Ly6C^{int}$, $Ly6G^{hi}$, CD11b+), monocytes ($Ly6C^{hi}$, $CD11b^{hi}$); NK cells ($NK1.1^{+}$, $TCR\beta^{neg}$), CD4 T cells ($TCR\beta^{+}$, $CD4^{+}$, $CD8^{-}$), and CD8 T cells ($TCR\beta^{+}$, $CD4^{+}$, $CD8^{-}$) (mean±SD; n=4-5 mice timepoint; data

representative of 3 independent experiments). F) Kinetics of adoptively transferred antigen specific $CD8^+$ OT-I T cell expansion in the OB, draining mandibular and superficial cervical LNs, and spleen after intranasal VSV infection. OT-I cells were defined as LIVE, $CD45.1^+$, $CD8^+$, $mTomato^+$ (mean±SD; n=4-5 mice/timepoint; 2 independent experiments).

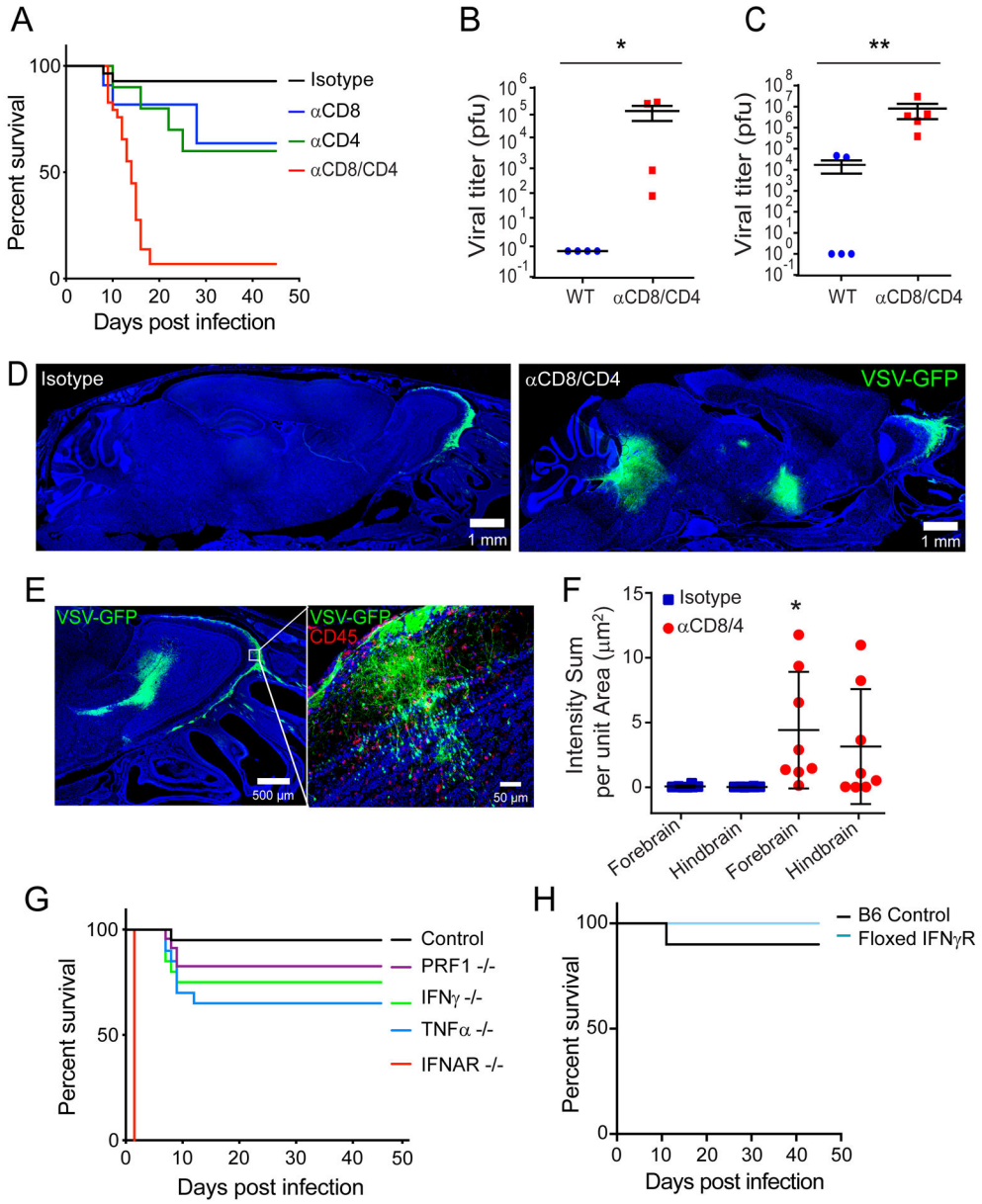

Figure 3. T cells prevent fatal VSV neuroinvasion after intranasal infection.

A) Survival curves of isotype control, αCD4, αCD8, or αCD8 / αCD4 treated mice following intranasal VSV infection (n=28 mice for isotype; n=10 for αCD4 depleted, p=0.0183; n=11 for αCD8 depleted, p=0.0263; n=31 mice for αCD8/4 depleted, p<0.0001; 2 independent experiments). B, C) Viral titers from the olfactory bulb (B) and remaining cerebrum (C) of isotype control or T cell depleted mice 8 days after intranasal VSV infection (n=4 mice per group; 2 independent experiments; *p=0.0286, **p=0.008). Black lines denote mean±SD. D) Representative confocal micrographs of sagittal brain sections (see Figure S1B) from an isotype control (left panel) or T cell depleted mouse (right panel) 8 days after intranasal VSV-eGFP infection. E) Representative confocal micrographs of viral escape from the glomerular layer within T cell depleted OBs after VSV-eGFP infection. F) Quantification of VSV-eGFP signal in the forebrain and hindbrains of isotype control or T

cell depleted animals (n=8 per group; 3 independent experiments; *p=0.02). Black lines denote mean±SD. G) Survival curves for VSV-OVA infected control, antibody treated mice and genetically deficient mouse strains (n=40 mice for control; n=20 for TNFα−/−, p<0.0021; n=9 for IFNAR−/−, p<0.0001; n=20 for IFNγ−/−, p=0.02; n=23 for PRF1−/−; p=0.1039; data are pooled from 6 independent experiments). H) Survival curves for control and floxed IFNγR mice infected intranasally with VSV-iCre (n=10 mice for control; n=9 mice for floxed IFNγR; p=0.3657; 2 independent experiments).

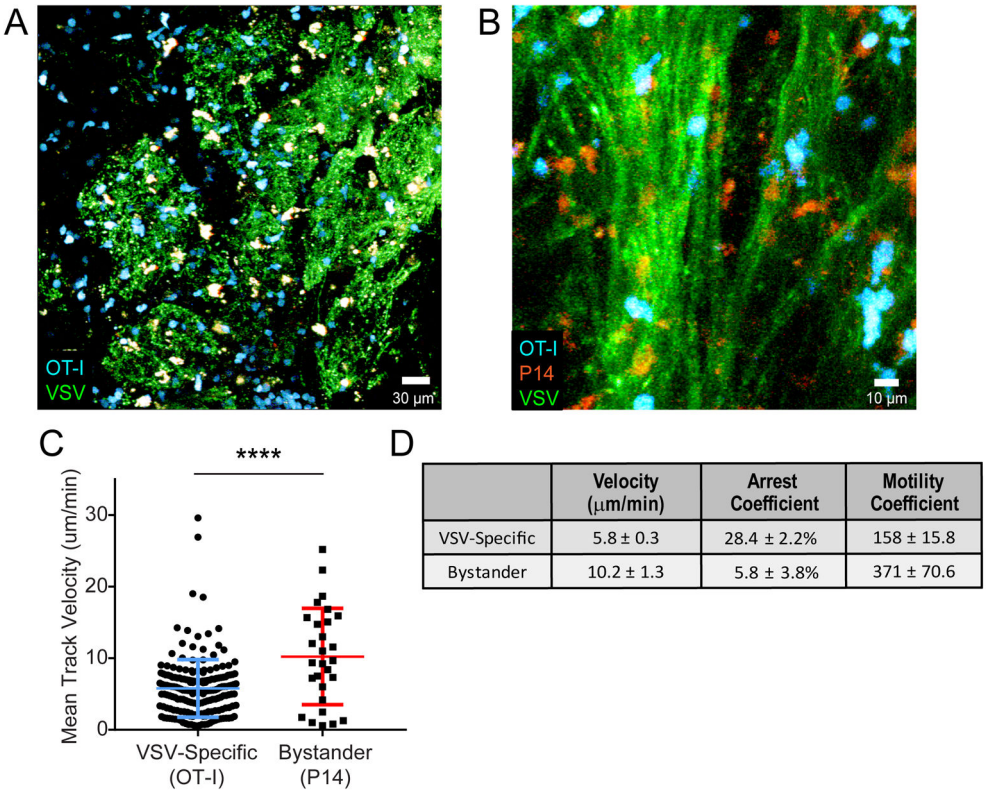

	Velocity (μm/min)	Arrest Coefficient	Motility Coefficient
VSV-Specific	5.8 ± 0.3	28.4 ± 2.2%	158 ± 15.8
Bystander	10.2 ± 1.3	5.8 ± 3.8%	371 ± 70.6

Figure 4. Antiviral CTLs exhibit decreased motility within the virally infected OB.

A) Representative image from an intravital imaging experiment depicting adoptively transferred virus-specific OT-I T cells (cyan) within the VSV-GFP (green) infected OB glomerular layer at day 7 post-infection. B) Representative image from a two-photon imaging experiment showing VSV-specific OT-I T cells (blue) and LCMV-specific P14 T-cells (red) traveling along VSV-eGFP (green) infected nerve fibers in the OB outer nerve layer. Mice were co-infected with VSV-eGFP and VSV-OVA for this experiment. C) Mean track velocity of VSV-specific OT-I T cells and LCMV-specific P14 T cells in day 7 VSV-infected OB (n=4 mice; 305 OT-I T cells and 57 P14 T cells; ****$p<0.0001$). Colored horizontal lines denote mean±SD. D) Motility analysis comparing average track velocities, arrest coefficients and motility coefficients for VSV specific OT-I T cells relative to bystander LCMV-specific P14 T cells within the infected OB at day 7 (from the same experiments as above; n=4 mice; average velocity $p<0.0001$, arrest coefficient $p=0.003$, motility coefficient $p<0.0001$).

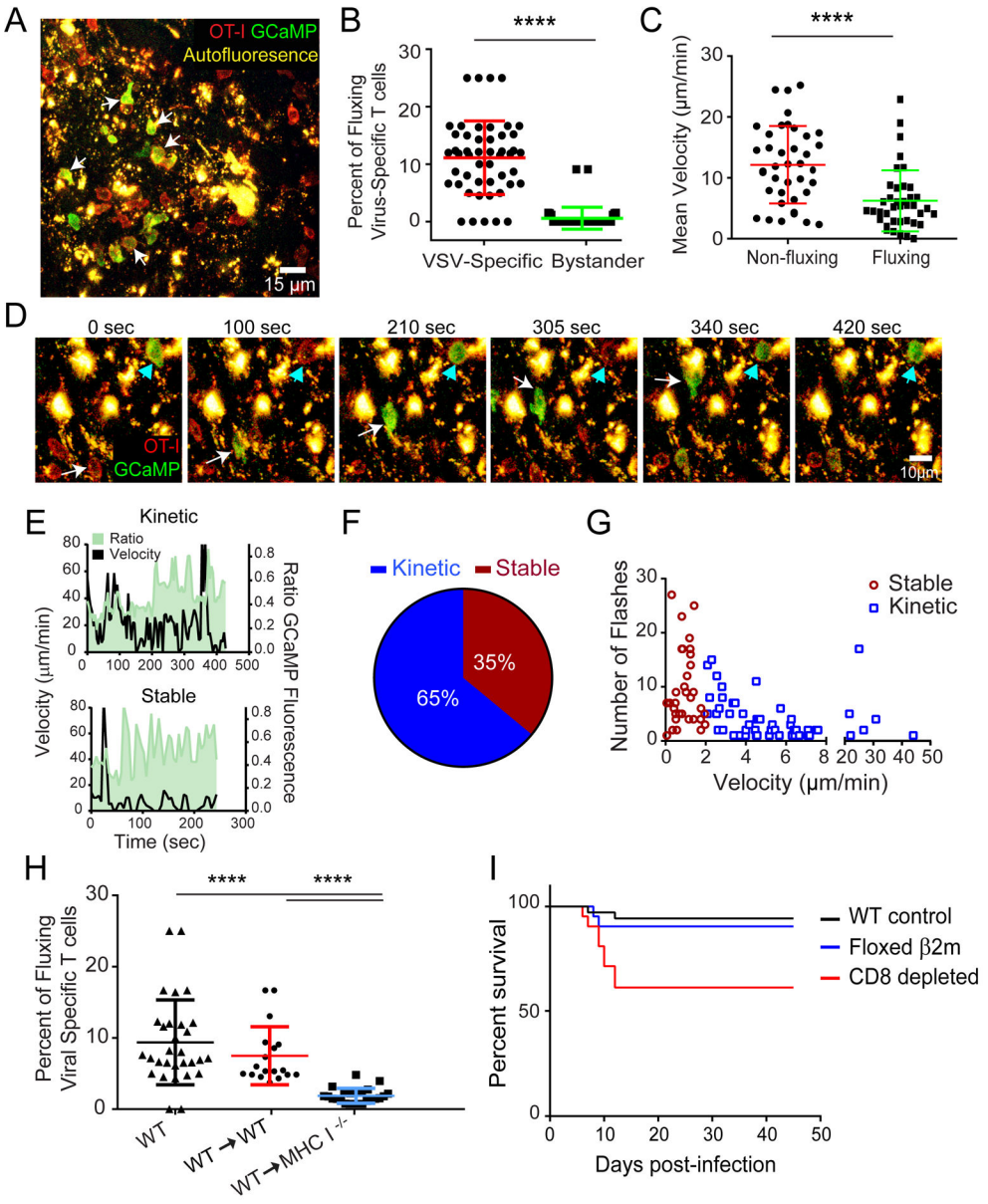

Figure 5. Antiviral CTL engage antigen on an uninfected CNS resident cell type.

A) A representative image from a two-photon imaging experiment shows OT-I mTomato+ GCaMP6s+ T cells in day 6 VSV-OVA infected OB. B) Calcium flux frequency of VSV-specific OT-I mTomato+ GCaMP6s+ Tcells compared with calcium flux frequency in bystander LCMV-specific P14 mTomato+ GCaMP6s+ T cells within VSV-OVA infected OB (n=4 mice; 6 time periods sampled per mouse; 24 OT-I T cells, 20 P14 T cells; ****p<0.0001). Colored horizontal lines denote mean±SD. C) Mean velocities of calcium fluxing vs. non fluxing OT-I mTomato+ GCaMP6s+ T cells within VSV-OVA infected OB (n=3 mice; 39 OT-I T cells; ****p<0.0001). Colored horizontal lines denote mean±SD. D) A representative time lapse from an intravital imaging experiment shows two different OT-I+ mTomato+ GCaMP6s+ T cells fluxing calcium (green) upon interaction with autofluorescent cells (yellow) within the VSV-OVA infected OB at day 6. The white arrow

denotes a T cell engaged in a kinetic fluxing behavior, whereas the cyan arrowhead denotes a stably arrested T cell fluxing calcium. E) Calcium and motility profiles for representative OT-I kinetic (upper panel, velocity of >2μm/min) and stable (lower panel, <2μm/min) interactions. F) Frequency of kinetic and stable calcium flux events in virus-specific OT-I T cells within the OB 6 days after VSV-OVA infection [(n=4 mice; 99 OT-I T cells total: 64 kinetic (>2μm/min) and 35 stable (<2μm/min)]. G) Number of calcium flux events as a function of velocity during kinetic and stable virus-specific OT-I T cells interactions in OB at day 6 (n=4 mice; 99 OT-I T cells total, same as above; p=0.001). H) Calcium flux frequency of OT-I mTomato+ GCaMP6s+ T cells within wild type (WT) non-chimeric, control bone marrow chimeric, and MHC class I deficient bone marrow chimeric mice (n=4 mice; 6 timepoints sampled per movie; ****p<0.0001). Horizontal lines denote mean±SD. I) Survival curves for WT (n=33 mice), floxed β2M (n=19 mice), and αCD8 depleted WT mice (n=13 mice) intranasally infected with VSV-iCre (p=0.0016 for WT vs αCD8, p=0.2825 for WT vs β2M, p=0.0347 floxed β2M vs. αCD8)

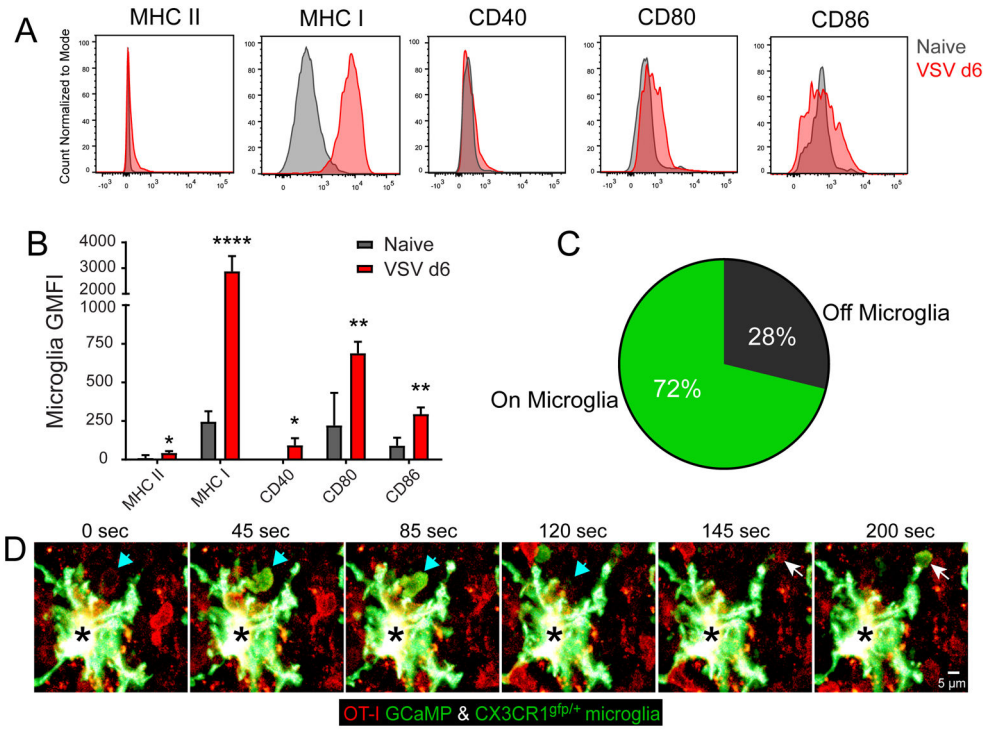

Figure 6. Microglia elicit antigen specific calcium flux from antiviral CTL.

A) Representative flow cytometric histograms of OB microglia show surface molecule expression 6 days after VSV infection (red) compared with naïve OB microglia (gray). Microglia were defined as Thy1.2- CD11b+ Ly6C- Ly6G- CD45int. B) Quantification of surface molecule geometric mean fluorescent intensity (GMFI) on OB microglia 6 days after VSV infection vs. naïve OB microglia. GFMI data for each surface marker are plotted as the mean±SD after subtracting the isotype control antibody GMFI (n=4 mice per group; 2 independent experiments; *p<0.05, **p<0.01, ****p<0.0001). C) Pie chart representing the frequency of all VSV-specific OT-I T cell calcium flux events observed by two-photon microscopy in contact or not in contact with CX3CR1$^{gfp/+}$ OB microglia in day 6 post-VSV-OVA infected bone marrow chimeric mice (i.e., CX3CR1$^{gfp/+}$ mice with C57BL/6J bone marrow) (n=5 mice; 9 movies; 61 time points; 4 independent experiments: p<0.0001). D) A representative time lapse from a two-photon imaging experiment shows an OT-I mTomato+ GCaMP6s+ T cells in a day 6 VSA-OVA infected CX3CR1$^{gfp/+}$ bone marrow chimera. Arrows (white and cyan) denote two virus-specific OT-I T cells fluxing calcium upon engagement of a single CX3CR1$^{gfp/+}$ microglia (black asterisk) in the infected OB.

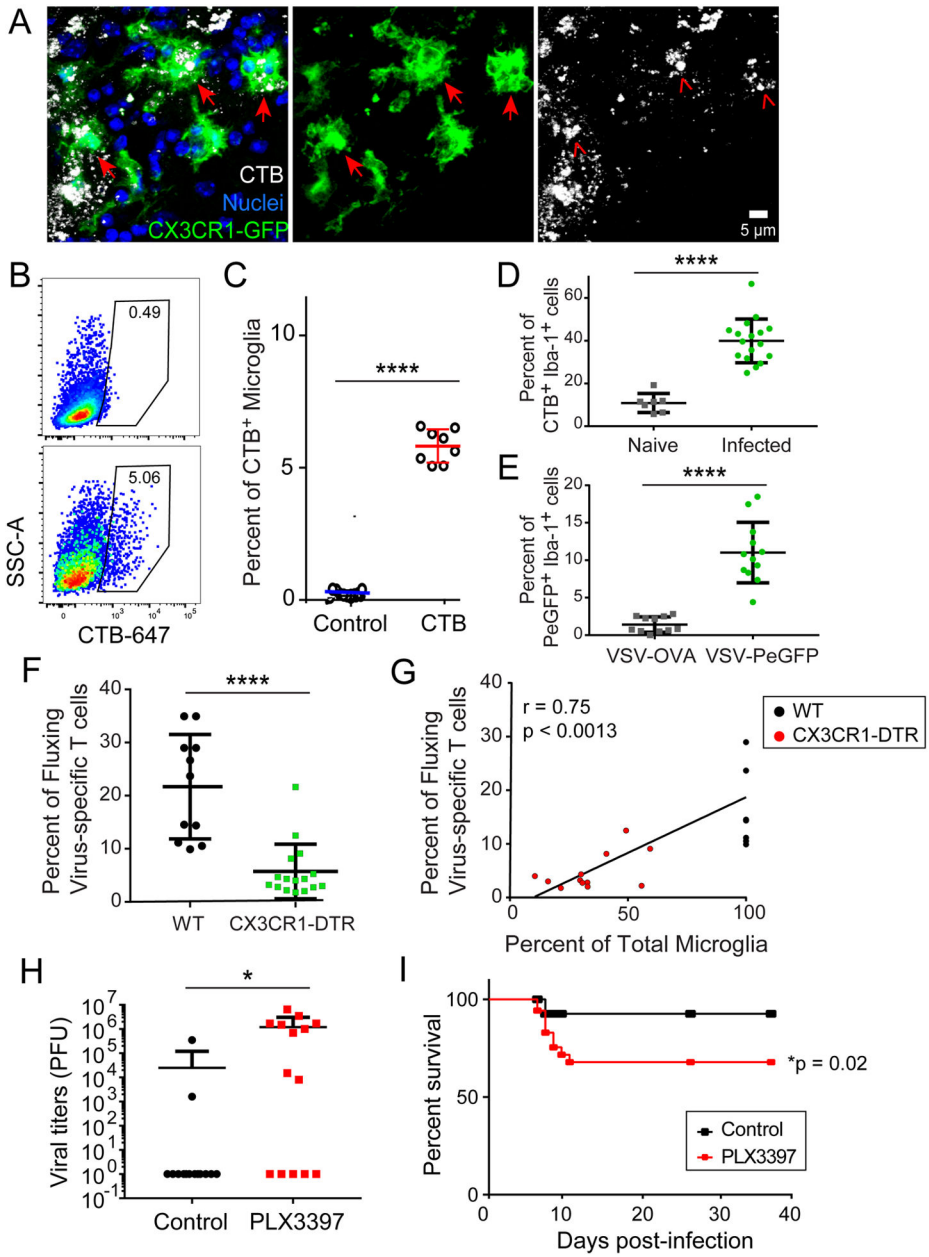

Figure 7. Microglia acquire and present antigen from virus-infected neurons to drive protective antiviral CTL responses.

A) Representative confocal micrographs of OB microglia (green) containing fragments of OSNs labeled with cholera toxin B (CTB, white) 10 hours prior to VSV infection. Images were captured at day 6 post-infection. B) Representative FACS plots of microglia (Thy1.2−, Cd11b+, Ly6C/G−, CD45int) from CTB-treated control (top) or day 6 VSV-infected mice (bottom). C) Quantification of CTB containing microglia frequencies. Values are normalized to VSV-infected mice without CTB to control for autofluorescence (7 mice per group; 2 independent experiments; ****p<0.001). Horizontal lines denote mean±SD. D) Frequency of microglia containing CTB within the OB glomerular layer of day 6 VSV infected mice as determined by quantification of confocal images. Values are normalized to VSV-infected

mice without CTB to control for autofluorescence (n=4 mice per group; n= 17 fields for day 6, 7 fields for naïve; ****p<0.001). Horizontal lines denote mean±SD. E) Frequency of GFP + microglia within the OB glomerular layer 6 days after VSV-PeGFP infection as determined by quantification of confocal images. Non-fluorescent VSV-OVA was used as a control (n=3 mice per group; n=12 fields for VSV-PeGFP, n=11 fields for VSV-OVA; ****p<0.0001). Horizontal lines denote mean±SD. F) Intravitally imaged calcium flux frequency of VSV-specific OT-I mTomato+ GCaMP6s+ T cells in wild type (WT) control vs. CX3CR1-CreER x ROSA $Stop^{fl/fl}$ DTR microglia depleted mice on day 6 post-VSV-OVA infection (n=6 control mice per group, 11 movies; n=7 mice microglia depleted mice per group, 16 movies; ****p=<0.001). Horizontal lines denote mean±SD. G) Calcium flux frequency of VSV-specific OT-I mTomato+ GCaMP6s+ T cells in control or CX3CR1-CreER x ROSA $Stop^{fl/fl}$ DTR microglia depleted animals as a function of microglia depletion efficiency (Pearson's r=0.753, p<0.0013). H) Viral titers in the brains of control vs. PLX3397 treated animals on day 7 post-VSV infection (14 mice per group from 3 pooled independent experiments; *p=0.0265). Horizontal lines denote mean±SD. I) Survival curve for control vs. PLX3397-treated VSV-infected mice (n=36 mice for control; n=35 mice for PLX3397; p=0.0201).